Preprints.org

Article

Not peer-reviewed version

Inexpensive Methods to Study the Radical Induced Degradation of Anion-Exchange Membranes

Panna Solyom , Thomas Nauser , Tamas Nemeth *

Posted Date: 3 September 2025

doi: 10.20944/preprints202509.0371.v1

Keywords: fuel cells; electrolysers; anion exchange membranes; radical reactions; photochemical reactions

Preprints.org is a free multidisciplinary platform providing preprint service that is dedicated to making early versions of research outputs permanently available and citable. Preprints posted at Preprints.org appear in Web of Science, Crossref, Google Scholar, Scilit, Europe PMC.

Copyright: This open access article is published under a Creative Commons CC BY 4.0 license, which permit the free download, distribution, and reuse, provided that the author and preprint are cited in any reuse.

Preprints.org (www.preprints.org) | NOT PEER-REVIEWED | Posted: 3 September 2025 doi:10.20944/preprints202509.0371.v1

Disclaimer/Publisher's Note: The statements, opinions, and data contained in all publications are solely those of the individual author(s) and contributor(s) and not of MDPI and/or the editor(s). MDPI and/or the editor(s) disclaim responsibility for any injury to people or property resulting from any ideas, methods, instructions, or products referred to in the content.

Article

Inexpensive Methods to Study the Radical Induced Degradation of Anion-Exchange Membranes

Panna Solyom [1], Thomas Nauser [2] and Tamas Nemeth [1,*]

[1] Panna Solyom Department of Sustainable Energy Technology SINTEF AS 7034 Trondheim, Norway

[2] Laboratory of Inorganic Chemistry ETH Zurich Vladimir-Prelog-Weg 1, 8093 Zurich, Switzerland

* Correspondence: tamas.nemeth@sintef.no

Abstract

We adapted two photochemical methods to generate radicals and assess their impact on anion exchange membrane stability, independent of base-induced degradation. By exposure of aqueous solutions of potassium nitrite or suspensions of TiO_2 to UV-light at 365 nm, we generated hydroxyl radicals or a combination of hydroxyl and superoxide radicals. The methods' applicability to anion exchange membranes (AEMs) is demonstrated on three commercial AEMs: PiperION-40, FM-FAA-3-PK-75, and PNB-R45. Changes in ion-exchange capacity, along with FT-IR, and NMR analyses revealed significant degradation in thinner, non-reinforced membranes, while thicker and reinforced membranes showed greater resistance. We attribute this to the limited penetration depth of highly reactive radicals into the membrane. Both methods are practical and inexpensive tools for benchmarking AEM stability against radical attack.

Keywords: fuel cells; electrolysers; anion exchange membranes; radical reactions; photochemical reactions

Introduction

Energy security and global warming have become a fundamental challenge of humanity. Global efforts are increasingly focused on replacing traditional fossil fuels with renewable energy sources and advancing electrochemical technologies for efficient energy storage and conversion. Water electrolysers (ELs) and fuel cells (FCs) are in the centre of significant attention as promising devices to balance the seasonality of renewable energy production. FCs, which efficiently convert the chemical energy of high-density fuels like hydrogen directly into electricity with zero emissions, offer a promising solution to decarbonize the transport sector, a major contributor to global warming and responsible for nearly one-third of global greenhouse gas emissions [1].

The high capital expenditure (CAPEX) associated with state-of-the-art proton exchange membrane (PEM) FCs and ELs stands as an obstacle before widespread commercialization. It is caused by the use of platinum group metal (PGM) catalysts and perfluorinated membranes [2]. As a result, there is a growing interest in complementary anion exchange membrane (AEM) technology, which operates under alkaline conditions and offers several advantages over PEMs: 1) kinetically more favorable oxygen evolution (OER) and reduction reactions (ORR) that reduces activation losses, 2) the possibility to use inexpensive non-precious metal catalysts, 3) sustainable membrane alternatives to traditional perfluorinated polymers, and 4) the use of inexpensive cell components due to the less corrosive operating environment [3].

However, the wide-spread application of both AEMFCs and AEMWEs is currently hindered by the rapid degradation of AEMs under alkaline conditions, this challenge is further exacerbated at low hydration levels [4]. In PEMs chemical degradation is mainly caused by electrophilic attack of oxidizing radicals formed during FC operation [5]. In AEMs, however, it is predominantly caused by the nucleophilic attack of OH^- [6]. Several OH^--induced degradation pathways for AEMs have been proposed, including (1) *Hofmann* elimination, (2) nucleophilic substitution, and (3) the formation of

© 2025 by the author(s). Distributed under a Creative Commons CC BY license.

Preprints.org (www.preprints.org) | NOT PEER-REVIEWED | Posted: 3 September 2025 doi:10.20944/preprints202509.0371.v1

ylides, which may undergo further rearrangement via *Stevens* or *Sommelet-Hauser* mechanisms [6]. These detrimental processes can occur simultaneously, significantly compromising membrane stability and prompting extensive research efforts aimed at enhancing the alkaline durability of AEMs.

Several studies have reported accelerated degradation under oxygen-saturated conditions, suggesting that reactive oxidising species (ROS) play a significant role in the degradation mechanisms of AEMs. Advancements in polymer backbones, quaternary ammonium headgroups, and crosslinking strategies have brought about a significant improvement in the alkaline stability of AEMs, however, strategies to improve the radical-induced degradation remain limited [6]. *Parrondo* et al. were the first to observe a significantly higher loss in ion-exchange capacity during ex-situ stability tests of poly(*p*-phenylene oxide)-based AEMs performed under oxygen saturated conditions compared to nitrogen degassed ones, highlighting the detrimental role of oxidative stress in AEM degradation [7]. Experiments involving spin trapping and use of a fluorescent dye are interpreted by time-dependent formation of various ROS, such as $HO^{\bullet}$, $HOO^{\bullet}$ and $O_2^{\bullet-}$ [7,8].

The ex-situ stability test conducted by *Espiritu* et al. also indicates increased IEC loss in vinylbenzyl chloride-grafted low-density polyethylene-based AEMs when exposed to oxygen [9].

Wierzbicki and colleagues were the first to detect in-situ radical formation in various AEMs by operating a micro-AEM-FC within an Electron Paramagnetic Resonance (EPR) setup. This enabled spin trapping of $HO^{\bullet}$ and $HOO^{\bullet}$ radicals on the cathode side and $H^{\bullet}$ radicals on the anode side [10]. Subsequent experiments revealed that radical formation occurs for both PGM-based and PGM-free electrocatalysts [11]. Under the premise that radicals are involved in the degradation of AEMs, it becomes essential to evaluate the ex-situ stability of novel AEMs before subjecting them to time- and resource-intensive in-device testing.

To assess the alkaline stability of AEM headgroups or fabricated AEMs, a widely adopted approach involves exposing the materials to concentrated alkaline solutions, typically 1–12 M potassium hydroxide (KOH) or sodium hydroxide (NaOH), at elevated temperatures, i.e., 80–160 °C [12].

In contrast, ex-situ degradation tests of PEMs, where degradation is driven by radicals, *Fenton*'s reaction is the most common method to form oxidising radicals, $HO^{\bullet}$ and $HOO^{\bullet}$ via reactions (1) – (3) and evaluate stability.

$$Fe^{2+} + H_2O_2 \rightarrow Fe^{3+} + HO^{\bullet} + OH^- \quad (1)\ E°(HO^{\bullet}, H^+/H_2O) = 2.73\ V$$

$$HO^{\bullet} + H_2O_2 \rightarrow H_2O + HOO^{\bullet} \quad (2)\ E°(HOO^{\bullet}, H^+/H_2O_2) = 1.46\ V$$

$$Fe^{3+} + H_2O_2 \rightarrow Fe^{2+} + HOO^{\bullet} + H^+ \quad (3)$$

While it may seem straightforward to subject AEMs to Fenton's test to benchmark oxidative stability [13]. at pH values above 5, highly oxidizing Ferryl radicals form rather than $HO^{\bullet}$ and $HOO^{\bullet}$ [14,15]. Reactivity and selectivity differ between Ferryl and $HO^{\bullet}$. Fenton chemistry, therefore, promotes misleading results in the study of $HO^{\bullet}$ radical-mediated degradation of AEMs.

Alternative approaches to generate radicals include thermal decomposition of dilute aqueous H_2O_2 solutions at elevated temperatures [16]. or using UV activation. There are several limitations with these methods [17]. First, thermal decomposition of H_2O_2 is not an efficient way to generate radicals [18]. While radical formation is possible via reaction (4), at elevated temperatures the process is dominated by non-radical thermal decomposition pathways, reaction (5). Second, while UV activation of H_2O_2 can effectively generate radicals, it requires irradiation at wavelengths below 300 nm. At these wavelengths direct photochemistry of aromatic AEMs will certainly be non-negligible and may even constitute the main reaction pathway.

$$H_2O_2 \rightarrow 2\ HO^{\bullet} \quad (4)\ \text{radical path}$$

$$H_2O_2 \rightarrow\rightarrow HO^{\bullet} \quad (5)\ \text{non-radical path}$$

A recently developed protocol enables the simultaneous assessment of base- and radical-induced degradation of AEMs by immersion in oxygen-saturated aqueous alkaline solutions at elevated temperatures [19]. While this method offers a more realistic simulation of operational conditions, it presents several limitations. First, the rate of radical formation is highly dependent on the concentration of dissolved oxygen. It decreases with both increasing temperature and hydroxide

© 2025 by the author(s). Distributed under a Creative Commons CC BY license.

Preprints.org (www.preprints.org) | NOT PEER-REVIEWED | Posted: 3 September 2025 doi:10.20944/preprints202509.0371.v1

concentration, due to the salting-out effect [20]. Second, because the protocol uses concentrated hydroxide solutions, it is not possible to distinguish between base-induced degradation and radical-induced degradation.

The concept of water radiolysis as a technique for selective production of specific radical species, using pulse- [21]. gamma- or beta- irradiation [22], is described in the literature in detail. These techniques allow for precise and quantitative control over radical formation, making them valuable tools for mechanistic studies. However, their application is limited by accessibility and costs, as they require specialized infrastructure which is unavailable in most research environments.

We recognized a need within the AEM research community for basic ex-situ degradation testing methods that are robust, affordable and accessible for standard laboratories. These should generate radical species representative of those produced in AEM FCs or ELs.

We adapt two known photochemical methods to generate radical species [23,24]. The effect of these treatments on AEMs is characterized. Both approaches rely on equipment that is either inexpensive or readily available in standard synthetic laboratories, making them highly accessible. Their practical applicability for ex-situ degradation studies will be demonstrated and discussed based on three commercially available, state-of-the-art AEMs: PiperION®-40 (PiperION), FM-FAA-3-PK-75 (Fumasep), and PNB-R45 (Polynorbornene).

Results and Discussion

Photochemical Generation of Radicals

The speciation and reactivity of radicals relevant to AEM FCs and ELs depends on pH. The pK_a of $HO^\bullet$ is 11.9 [24], therefore, both its protonated and deprotonated forms, $O^{\bullet-}$, are present under the alkaline conditions of an AEM FC or EL, with the latter dominating. In contrast, the pK_a of $HOO^\bullet$ is 4.8 [25], thus, under strongly alkaline conditions it is present in its deprotonated form $O_2^{\bullet-}$. We focus, therefore, on selective production of $HO^\bullet/O^{\bullet-}$ and $O_2^{\bullet-}$ in presence of AEMs. Photolysis of nitrite produces $HO^\bullet$, reaction (6).

$$NO_2^- + H_2O + h\nu \rightarrow HO^\bullet + NO^\bullet + OH^- \qquad (6)$$

A critical review of the corresponding photochemistry was published by *Mack and Bolton* [26]. *Takeda* et al. recently showed a practical application of that reaction using dilute aqueous solutions of nitrite and a 365 nm UV-LED [23]. The production rate of $HO^\bullet$ was estimated by the reaction with terephthalate, a highly sensitive and water-soluble fluorescent probe. Nitrite concentrations were limited to the micromolar range because, while nitrite serves as a photochemical source of hydroxyl radicals, reaction (6), it also acts as a highly efficient $HO^\bullet$ scavenger, reaction (7), with a reported rate constant of $k = 8 \times 10^9$ $M^{-1}s^{-1}$ [27].

$$NO_2^- + HO^\bullet \rightarrow NO_2^\bullet + OH^- \qquad (7)$$

Maintaining nitrite concentrations in the micromolar range minimizes the effect of reaction (7). However, it also lowers the maximum achievable steady-state concentration of $HO^\bullet$, as photolysis, reaction (6), is proportional to the absorption of photons. The latter is proportional to the availability and molar absorptivity of nitrite as a photochemical precursor.

The stress-test of AEMs, on the other hand, requires elevated concentrations of $HO^\bullet$. We used 4.5 mM benzoic acid (BA) to probe for photochemically formed hydroxyl radicals, reaction (8), and observed the yield of reaction (8) as a function of the nitrite concentration which was varied between 0.1 mM and 2 mM.

$$BA + HO^\bullet \rightarrow \text{Products} \qquad (8)$$

We calculated the pseudo-first-order rate constants (k') for the reactions of hydroxyl radicals with nitrite and with BA by multiplying the reported second-order rate constants (k) with the respective solute concentrations. The resulting k' values are proportional to the production rates of the respective processes, and their ratio is proportional to the relative product yields of the competing reactions (7) and (8), under various conditions, Table 1.

© 2025 by the author(s). Distributed under a Creative Commons CC BY license.

Preprints.org (www.preprints.org) | NOT PEER-REVIEWED | Posted: 3 September 2025 doi:10.20944/preprints202509.0371.v1

Table 1. Competing reactions for the hydroxyl radicals at different nitrite concentrations.

Reaction	Reactant	k / $M^{-1}s^{-1}$	Conc / mM	k' / s^{-1}	Yield / %
(7)	NO_2^-	8×10^9	0.1	8×10^5	8
(8)	BA	2×10^9	4.5	9×10^6	92
(7)	NO_2^-	8×10^9	0.6	4.8×10^6	35
(8)	BA	2×10^9	4.5	9×10^6	65
(7)	NO_2^-	8×10^9	1	8×10^6	47
(8)	BA	2×10^9	4.5	9×10^6	53
(7)	NO_2^-	8×10^9	2	1.2×10^7	64
(8)	BA	2×10^9	4.5	9×10^6	36

While approximately 92% of the formed $HO^\bullet$ react with BA at a low nitrite concentration of 0.1 mM, only 36% will do so at a high nitrite concentration of 2 mM. The higher nitrite concentration significantly increases the production rate of $HO^\bullet$ radicals (up to 20 times), which also increases BA degradation despite the lower relative yield of reaction (8).

The reaction model was tested using 4.5 mM BA in 0.1 mM NaOH (pH 10) and nitrite concentrations in the range of 0.6–2 mM. Experiments were performed under continuous irradiation at 365 nm. To selectively focus on radical-induced degradation, with limited influence from HO^-, irradiations were conducted at 80 °C and pH 10. BA degradation was monitored by its absorbance at 227 nm, **Figures 1 and 2.**

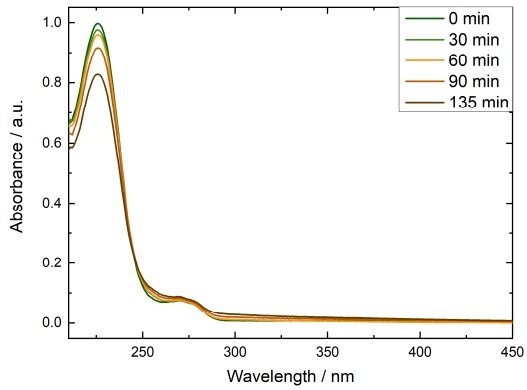

Figure 1. Absorption spectra after 0, 30, 60, 90 or 135 min of irradiation at 80 °C, normalized to the maximum absorbance of BA, measured in 4.5 mM benzoic acid solutions that contained 0.1 mM NaOH and 2 mM potassium nitrite.

The formation of $HO^\bullet$ can be assessed by photochemical probes via quantification of specific reaction products [28], such as hydroxylated derivatives of BA. However, this method may underestimate $HO^\bullet$ formation if multiple parallel reaction pathways are present and the product concentrations are low. A more reliable, albeit less selective, alternative is to monitor the overall consumption of BA.

In all cases we observed a decrease of BA concentration over time. At shorter irradiation times BA degradation was larger at lower nitrite concentrations, after 135 min of continuous irradiation,

© 2025 by the author(s). Distributed under a Creative Commons CC BY license.

Preprints.org (www.preprints.org) | NOT PEER-REVIEWED | Posted: 3 September 2025 doi:10.20944/preprints202509.0371.v1

the average degree of degradation increased with increasing nitrite concentration, **Figure 2**. To inflict appreciable damage to commercial AEMs, we chose to use a higher nitrite concentration of 2 mM. The controls showed no BA degradation in the absence of irradiation or nitrite.

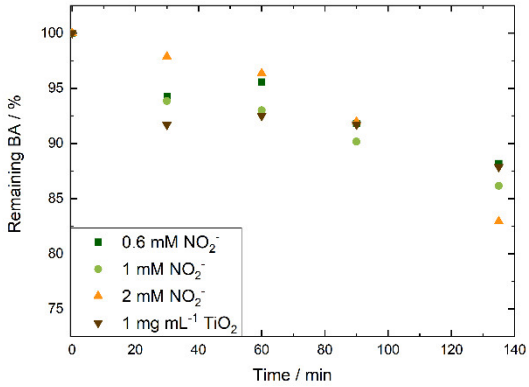

Figure 2. Change in absorbance at 227 nm observed in irradiated 4.5 mM benzoic acid solutions that contained 0.1 mM NaOH and 0.6 (orange triangles), 1 (green circles) or 2 mM (green squares) potassium nitrite or 1 mg mL^{-1} TiO_2 (brown triangles). Irradiation took place at 80 °C, UV-vis was recorded at room temperature. Averages of three repeats are shown.

Not only $HO^{\bullet}$ but also $O_2^{\bullet-}$ is relevant for the degradation of AEM systems. Since nitrite irradiation forms $HO^{\bullet}$ and $NO^{\bullet}$, we looked for alternative approaches that generate $O_2^{\bullet-}$ instead. We adapted a photocatalytic method which forms radicals from TiO_2 suspension [24]. Various ROS are generated in photocatalytic processes on TiO_2 surface when exposed to UV irradiation, reactions (9)-(11). Conduction band electrons react with dissolved oxygen forming superoxide radicals, and valance band holes react with water to produce $HO^{\bullet}$. Radical generation is dependent on TiO_2 crystal phase. Anatase type TiO_2 is more efficient at radical generation than rutile due to better charge separation and enhanced absorption of intermediate species [29].

$$TiO_2 + h\nu \rightarrow e^-_{CB} + h^+_{VB} \quad (9)$$

$$e^-_{CB} + O_2 \rightarrow O_2^{\bullet-} \quad (10)$$

$$h^+_{VB} + H_2O \rightarrow HO^{\bullet} + H^+ \quad (11)$$

Irradiation with a 365 nm (3.4 eV) light source is sufficient to form radicals in a suspension of anatase-phase TiO_2, which has a band gap of approximately 3.2 eV [30]. Accordingly, we irradiated aqueous solutions containing 4.5 mM BA, 0.1 mM NaOH (pH 10) and anatase TiO_2 at 365 nm for 30, 60 90 and 135 min at 80 °C. At an optimized TiO_2 concentration of 1mg mL^{-1}, time-dependent degradation of BA was observed, **Figure 2**. In subsequent experiments, we implemented the two methods to evaluate the stability of commercial AEMs against radical attack.

Radical-Induced Degradation of AEMs

To evaluate and compare the two photochemical methods for studying radical-induced degradation of AEMs, we selected three commercially available, state-of-the-art AEMs: PiperION, Fumasep, and Polynorbornene, **Figure 3**. The structural diversity of these membranes is the basis to demonstrate the broad applicability of the methods. While PiperION and Fumasep feature aromatic backbones [31,32]. Polynorbornene is based on a non-aromatic structure [33]. Additionally, Fumasep and Polynorbornene incorporate mechanical reinforcement, whereas PiperION does not.

© 2025 by the author(s). Distributed under a Creative Commons CC BY license.

Preprints.org (www.preprints.org) | NOT PEER-REVIEWED | Posted: 3 September 2025 doi:10.20944/preprints202509.0371.v1

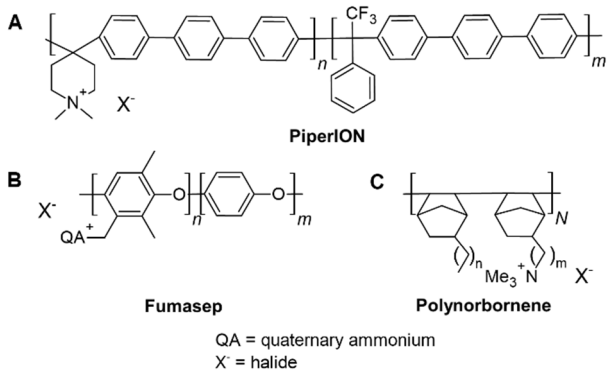

Figure 3. Reported structures of the AEMs investigated in this study.

Practical Considerations

Before subjecting the AEMs to degradation tests, all samples were converted to the hydroxide form by ion-exchanging three times in 1 M KOH. It is important to note that when membranes are in the halide form, common for commercial AEMs such as Polynorbornene or Fumasep, the generated $HO^{\bullet}$ radicals react diffusion controlled with the halides via reactions (12) and (13) [34,35]. PiperION is shipped in the bicarbonate form. The reported rate constant for the reaction between carbonate and $HO^{\bullet}$, reaction (14), is one order of magnitude slower [36]. Consequently, a portion of the generated $HO^{\bullet}$ will be consumed in these side reactions, reducing its availability for the primary reaction pathway. Formed $X_2^{\bullet-}$ and carbonate anion radicals are potent oxidants, however, not relevant for AEMs.

$$Br^- + HO^{\bullet} \rightarrow Br^{\bullet} + HO^- \quad (12)\ k = 1.1\times10^{10}\ M^{-1}s^{-1}$$

$$Br^- + Br^{\bullet} \rightarrow Br_2^{\bullet-} \quad (13)\ k = 1.2\times10^{10}\ M^{-1}s^{-1}$$

$$CO_3^{2-} + HO^{\bullet} \rightarrow CO_3^{\bullet-} + HO^- \quad (14)\ k = 4\times10^{8}\ M^{-1}s^{-1}$$

Accordingly, we performed all experiments with AEMs in the hydroxide form. Radical reactivity is known to be influenced by ionic strength [37]. Therefore, we used 0.333 M sodium sulfate to establish the same ionic strength as at pH 14, typical of the environment in AEM FCs and ELs.

Although the reaction rate constants between hydroxide and $HO^{\bullet}$ are also relatively high, reaction (15), the reaction product is $O^{\bullet-}$, i.e., the deprotonated form of $HO^{\bullet}$ that dominates under the highly alkaline conditions typical for AEMs (pH > 12) [38].

$$HO^- + HO^{\bullet} \rightarrow H_2O + O^{\bullet-}\ (15)\ k = 1.2\times10^{10}\ M^{-1}s^{-1}$$

Next, we reacted the solution-immersed AEMs with primary radicals that were produced by irradiating the solution of 2 mM nitrite, 0.1 mM NaOH and 0.333 M Na_2SO_4, or a suspension of 10 gL^{-1} TiO_2 in 0.1 mM NaOH and 0.333 M Na_2SO_4 at 365 nm for 30, 60 90 and 135 min.

Following irradiation, we performed a visual inspection of the AEM samples to assess their stability against radical attack, **Figures S1-S3**. We found that the colour of the PiperION samples darkened after prolonged irradiation with both methods, **Figure S1**. In contrast, a colour change was observed for both the Polynorbornene and Fumasep AEM samples only in the cases of the irradiated nitrite-containing solutions, **Figures S2-S3**.

Both chemical and mechanical degradation of ion-exchange membranes are strongly influenced by the presence of reinforcements and the material thickness. Thicker membranes generally exhibit a lower degree of degradation, as radicals penetrate less deeply, resulting in slower degradation rates. Additionally, reinforced membranes tend to better resist both mechanical and chemical degradation [39].

Accordingly, when we examined changes in IEC of the AEMs subjected to degradation tests, we observed a gradual decrease in IEC across all methods and membrane samples (Table 2). However, in the case of Fumasep, degradation was significantly suppressed. This can be attributed to the fact that this AEM was both reinforced and thicker than the other tested membranes, with a dry thickness

© 2025 by the author(s). Distributed under a Creative Commons CC BY license.

Preprints.org (www.preprints.org) | NOT PEER-REVIEWED | Posted: 3 September 2025 doi:10.20944/preprints202509.0371.v1

of 75 µm compared to 40 µm for PiperION and 45 µm for Polynorbornene. We found that Polynorbornene lost approximately 17% and 22% of its IEC after 135 min of continuous irradiation of the nitrite- and TiO_2-containing solutions, respectively. In contrast, PiperION exhibited IEC losses of approximately 18% and 46% under the same conditions. It was surprising that degradation of PiperION showed an "induction phase" with the TiO_2 model. Up to 90 minutes irradiation, there was almost no change in the IEC. However, during the next 45 minutes there was a loss of almost 50%. This observation was confirmed several times.

Table 2. Remaining ion-exchange capacity of the respective AEMs following the degradation tests.

Time / min	Remaining IEC [1] / %					
	Fumasep		Polynorbornene		PiperION	
	NO_2^-	TiO_2	NO_2^-	TiO_2	NO_2^-	TiO_2
0	100±2	100±4	100±1	100±1	100±1	100±1
30	96±3	96±1	91±6	100±4	93±3	97±1
60	90±2	89±4	83±4	97±7	94±2	99±<1
90	93±2	89±3	74±10	84±12	86±2	98±2
135	87±1	92±10	83±9	78±12	82±11	54±3

[1] IECs were normalized to the beginning-of-test IEC of each respective AEM type, averages of three measurements are shown.

To qualitatively assess AEM degradation, we compared the FT-IR spectra recorded before (BoT) and after 135 minutes of degradation, **Figure 4** and **Figures S4** and **S5**.

Consistent with the small change in IEC (Table 2), no significant structural changes could be observed in the reinforced Fumasep samples following the degradation tests (**Figure S4**). It is important to note that FT-IR measurements are semi-quantitative, and structural changes at the few-percent level may be difficult to detect.

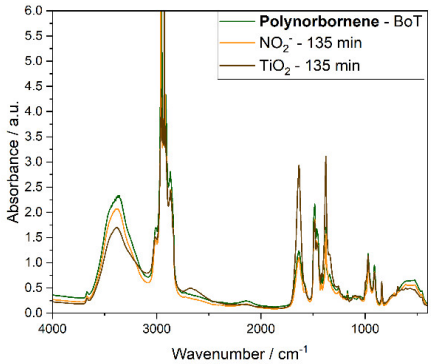

Figure 4. Transmission FT-IR spectra of Polynorbornene AEM samples before (BoT, green line) and after irradiation at 365 nm of the solution of 2 mM nitrite, 0.1 mM NaOH and 0.333 M Na_2SO_4 135 min (orange line), or the suspension of 10 $mgmL^{-1}$ TiO_2 in 0.1 mM NaOH and 0.333 M Na_2SO_4 for 135 min (brown line).

In contrast, the Polynorbornene samples exhibited structural changes, particularly in the absorbance bands associated with C–N stretching vibrations, specifically at 836, 910, 970, and 1076 cm^{-1} [33]. **Figure 4**. Additionally, changes in the peaks at 1486, 1637, 2146, and 2870 cm^{-1} suggest oxidative degradation of the polymer backbone and side chains, likely involving the formation of unsaturated and carbonyl-containing species. Both Fumasep and

© 2025 by the author(s). Distributed under a Creative Commons CC BY license.

Preprints.org (www.preprints.org) | NOT PEER-REVIEWED | Posted: 3 September 2025 doi:10.20944/preprints202509.0371.v1

Polynorbornene samples were insoluble in common deuterated solvents, which precluded quantitative NMR analysis.

In the case of PiperION AEM, increased absorbance at 1633, 1380, 2657, and 2940 cm^{-1} indicates oxidative degradation, likely involving the formation of unsaturated and carbonyl-containing species and side-chain fragmentation. Notably, significant structural changes were observed at these frequencies in samples irradiated in the presence of TiO_2 (**Figure S5**), whereas samples irradiated in the presence of nitrite showed minimal spectral changes.

Next, we performed NMR analysis to further analyse degradation of PiperION. Addition of a small amount of TFA served to separate the protonated piperidine signals and downfield shift the water signal. We compared the ratio of the integrals for the piperidinium ring and quaternary ammonium headgroup, peaks at 2.88 and 3.13 ppm, and of the aromatic protons between 6.7 and 8.2 ppm, **Figure 5**. Overlap of the water signal with the piperidinium protons at 3.4 ppm prevented integration of this latter peak. We found that the ratio of aliphatic-to-aromatic protons decreased in the case of both PiperION samples that were irradiated for 135 min in the presence of nitrite or TiO_2. This indicates loss of aliphatic protons, probably related to degradation of the quaternary ammonium headgroups, in good agreement with the ion-exchange capacity loss in Table 2. Moreover, we observed decreased solubility and pronounced brittleness in both degraded PiperION samples, which may indicate crosslinking [40].

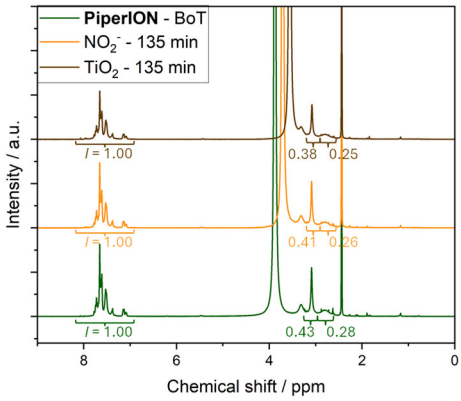

Figure 5. NMR spectra of PiperION AEM samples before (BoT, green line) and after irradiation at 365 nm of the solution of 2 mM nitrite, 0.1 mM NaOH and 0.333 M Na_2SO_4 135 min (orange line), or the suspension of 10 $mgmL^{-1}$ TiO_2 in 0.1 mM NaOH and 0.333 M Na_2SO_4 for 135 min (brown line).

Method Applicability to Compare AEMs

While both methods support the study of radical-induced degradation of AEMs, minimizing influence from HO^--mediated pathways, they exhibit limitations. In the case of the irradiation of nitrite-containing solutions, there is effective competition between nitrite and the AEMs for the generated $HO^\bullet$ radicals. As a result, nitrite concentrations must be kept relatively low. However, excessively low nitrite concentrations inherently restrict the steady-state concentration of $HO^\bullet$ that can be generated, thereby limiting the extent of AEM degradation. In the authors' opinion, using 2 mM nitrite offers a good balance between minimizing competition and maintaining sufficient radical generation for meaningful degradation. We note that at high oxygen concentrations, highly reactive $NO_2^\bullet$ radicals form via reaction (16) [41]. However, the high ionic strength established in our experiments, limited the availability of oxygen and minimised the interference of reaction (16).

$$O_2 + 2\ NO^\bullet \rightarrow 2\ NO_2^\bullet \qquad (16)\ k = 2.1\times10^6\ M^{-1}s^{-1}$$

© 2025 by the author(s). Distributed under a Creative Commons CC BY license.

Preprints.org (www.preprints.org) | NOT PEER-REVIEWED | Posted: 3 September 2025 doi:10.20944/preprints202509.0371.v1

In the case of TiO_2 suspensions, the rate of radical formation upon irradiation depends on both the crystal structure and the particle size [42]. We observed effective radical generation using anatase-type TiO_2 with mesh 325. Vigorous stirring of the suspension is essential to maintain the photochemical generation of radicals, as insufficient stirring may cause the TiO_2 particles to sediment, reducing their exposure to light and thus limiting reaction efficiency. In contrast, for radical generation from nitrite solutions, if the nitrite concentration remains uniform, stirring will not affect the quantum yield of radicals. Both methods of radical production show a larger impact on relatively thin AEMs, as our results show that thicker and reinforced membranes tend to degrade less. This is likely due to the limited penetration depth of radicals, which limits degradation in more robust membrane structures.

Conclusion

We implemented two literature methods to study the radical-induced degradation of AEMs. Both methods rely on photochemical generation of primary radicals: the UV-irradiation of solutions containing nitrite selectively forms $HO^{\bullet}/O^{\bullet-}$, while irradiation of TiO_2-containing suspensions generates both $HO^{\bullet}/O^{\bullet-}$ and $O_2^{\bullet-}$. After prolonged irradiation, i.e., at higher turnover of radicals, we observed an enhanced degree of membrane degradation in both methods. By performing the degradation tests at pH 10, we succeeded in deconvoluting base- and radical-induced degradation. Our findings may be exploited for benchmarking novel AEMs against radical stability and aid the design of next-generation AEMs that are stable under alkaline conditions and against radical attack.

Experimental Section

Chemicals and Reactants

Benzoic acid (>99.9%, EMSURE® ACS, Reag. Ph Eur), NaOH (>99%, pellets for analysis EMSURE®), potassium nitrite (ACS reagent, ≥96.0%) and anatase titanium(IV) dioxide (≥99%, 325 mesh) were purchased from Sigma Aldrich. The AEMs used in this study, PiperION®-40 (PiperION), FM-FAA-3-PK-75 (Fumasep), and PNB-R45 (Polynorbornene), were purchased from Fuel Cell store. AEMs were exchanged into the hydroxide form following the procedures of the supplier. During the irradiation experiments, 365 nm light sources with a rated power of 3 W (Alonefire SV98-365nm, Shenzen ShiWang Technolgy Co. Ltd.) were used, with the charging cable continuously connected. The light source was mounted on top of 25 mL transparent glass vials in such a way that it was positioned 1 cm from the surface of the solution.

Small molecule study: In the experiments involving potassium nitrite, aqueous solutions containing 4.5 mM BA in 0.1 mM NaOH (pH 10) and varying potassium nitrite concentration of 0.6–2 mM were irradiated for 30, 60, 90 or 135 min at 365 nm at 80 °C. In the experiments involving TiO_2, we irradiated at 80 °C aqueous solutions containing 4.5 mM BA, 0.1 mM NaOH (pH 10) and 1–10 mg mL^{-1} anatase TiO_2 at 365 nm for 30, 60 90 and 135 min.

AEM study: before the irradiation experiments, commercial AEMs were converted to the hydroxide form by ion-exchanging three times in 1 M KOH and subjected immediately to irradiation to minimize the ion-exchange to carbonate form. AEMs were placed in a solution of 2 mM nitrite, 0.1 mM NaOH and 0.333 M Na_2SO_4, or a suspension of 10 mg mL^{-1} TiO_2 in 0.1 mM NaOH and 0.333 M Na_2SO_4, and irradiated at 365 nm for 30, 60 90 and 135 min. Solutions were stirred at 80 °C at 400 rpm. Following the irradiation, the AEMs were placed in 1 M KOH, then washed successively in water and used directly to measure ion-exchange capacity.

Ion-exchange capacity (IEC) was measured by back titration of the membranes with 0.01 M KOH. AEM samples were placed into 1 M KOH solution for 1 h, washed successively with water, and placed in 0.01 M HCl solution for at least 4 h. Finally, the solutions were titrated with a standard 0.01 M KOH solution using a TitroLine® 5000 automatic titrator. Samples were dried in the oven at 80 °C for overnight and the dry weight was measured. The IEC (expressed as mmol g^{-1} dry polymer) was calculated according to the following equation:

© 2025 by the author(s). Distributed under a Creative Commons CC BY license.

Preprints.org (www.preprints.org) | NOT PEER-REVIEWED | Posted: 3 September 2025 doi:10.20944/preprints202509.0371.v1

$$IEC = \frac{V_{HCl} * C_{HCl} - V_{KOH} * C_{KOH}}{m_{dry}}$$

UV-vis measurements were performed using a Thermo Scientific Evolution 220 UV apparatus. An automatic background subtraction was done prior to data analysis. Fourier Transform Infrared Spectroscopy (FT-IR) measurements were performed using a Bruker vortex 80v apparatus. Measurements were performed under vacuum to suppress water absorption of the AEMs. Every measurement consisted of 20 scans that were averaged. Scanning was done from 400 to 4000 cm^{-1} with a spectral resolution of 2 cm^{-1}. An automatic background subtraction was done prior to data analysis. Changes in the chemical structure of PiperION samples were analysed by ^1H nuclear magnetic resonance (NMR, AVANCE NEO 400 MHz, Bruker, German) spectroscopy. The sample was dissolved in 500 µL DMSO-d_6 and 2 µL trifluoroacetic acid was added. Chemical shifts were referenced to the DMSO-d_6 solvent signal, 2.44 ppm.

Entry for the Table of Contents

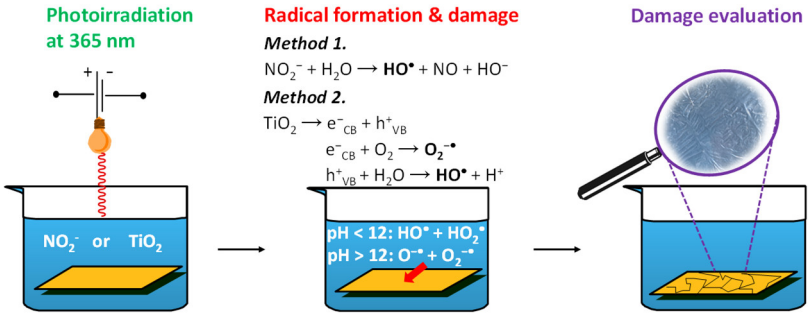

Caption:

Ex-situ methods for evaluating the radical stability of anion exchange membranes. Radicals were generated by irradiation of an aqueous potassium nitrite solution or a TiO_2 suspension, with the membranes immersed during exposure.

Author Contributions: T. Nemeth conceptualized this study, was responsible for the design of the experiments, the curation and analysis of data, and developed the methodology used in the degradation studies. P.V. Solyom was responsible for data curation and analysis of data. T. Nauser was essential for data curation. The authors express gratitude to L. C. Colmenares Rausseo for securing funding.

Acknowledgements: The authors are grateful for funding from SINTEF AS (grant no. 102033046 PoP-SEP funding scheme). This experimental work was performed in the Norwegian Fuel Cell and Hydrogen Centre, a research infrastructure supported by the Research Council of Norway under grant number 245678.

References

1. Wang, Y.; Yuan, H.; Martinez, A.; Hong, P.; Xu, H.; Bockmiller, F. R. Polymer Electrolyte Membrane Fuel Cell and Hydrogen Station Networks for Automobiles: Status, Technology, and Perspectives. *Advances in Applied Energy* **2021**, *2*, 100011. https://doi.org/10.1016/j.adapen.2021.100011.
2. Kim, M.; Lee, D.; Qi, M.; Kim, J. Techno-Economic Analysis of Anion Exchange Membrane Electrolysis Process for Green Hydrogen Production under Uncertainty. *Energy Conversion and Management* **2024**, *302*, 118134. https://doi.org/10.1016/j.enconman.2024.118134.
3. Grigoriev, S. A.; Fateev, V. N.; Bessarabov, D. G.; Millet, P. Current Status, Research Trends, and Challenges in Water Electrolysis Science and Technology. *International Journal of Hydrogen Energy* **2020**, *45* (49), 26036–26058. https://doi.org/10.1016/j.ijhydene.2020.03.109.
4. Willdorf-Cohen, S.; Mondal, A. N.; Dekel, D. R.; Diesendruck, C. E. Chemical Stability of Poly(Phenylene Oxide)-Based Ionomers in an Anion Exchange-Membrane Fuel Cell Environment. *J. Mater. Chem. A* **2018**, *6* (44), 22234–22239. https://doi.org/10.1039/C8TA05785K.

© 2025 by the author(s). Distributed under a Creative Commons CC BY license.

Preprints.org (www.preprints.org) | NOT PEER-REVIEWED | Posted: 3 September 2025 doi:10.20944/preprints202509.0371.v1

5. Gubler, L.; Dockheer, S. M.; Koppenol, W. H. Radical (HO • , H • and HOO •) Formation and Ionomer Degradation in Polymer Electrolyte Fuel Cells. *J. Electrochem. Soc.* **2011**, *158* (7), B755–B769. https://doi.org/10.1149/1.3581040.
6. Mustain, W. E.; Chatenet, M.; Page, M.; Kim, Y. S. Durability Challenges of Anion Exchange Membrane Fuel Cells. *Energy Environ. Sci.* **2020**, *13* (9), 2805–2838. https://doi.org/10.1039/D0EE01133A.
7. Parrondo, J.; Wang, Z.; Jung, M.-S. J.; Ramani, V. Reactive Oxygen Species Accelerate Degradation of Anion Exchange Membranes Based on Polyphenylene Oxide in Alkaline Environments. *Phys. Chem. Chem. Phys.* **2016**, *18* (29), 19705–19712. https://doi.org/10.1039/C6CP01978A.
8. Zhang, Y.; Parrondo, J.; Sankarasubramanian, S.; Ramani, V. Detection of Reactive Oxygen Species in Anion Exchange Membrane Fuel Cells Using In Situ Fluorescence Spectroscopy. *ChemSusChem* **2017**, *10* (15), 3056–3062. https://doi.org/10.1002/cssc.201700760.
9. Espiritu, R.; Golding, B. T.; Scott, K.; Mamlouk, M. Degradation of Radiation Grafted Hydroxide Anion Exchange Membrane Immersed in Neutral pH: Removal of Vinylbenzyl Trimethylammonium Hydroxide Due to Oxidation. *J. Mater. Chem. A* **2017**, *5* (3), 1248–1267. https://doi.org/10.1039/C6TA08232G.
10. Wierzbicki, S.; Douglin, J. C.; Kostuch, A.; Dekel, D. R.; Kruczała, K. Are Radicals Formed During Anion-Exchange Membrane Fuel Cell Operation? *J. Phys. Chem. Lett.* **2020**, *11* (18), 7630–7636. https://doi.org/10.1021/acs.jpclett.0c02349.
11. Wierzbicki, S.; Douglin, J. C.; Singh, R. K.; Dekel, D. R.; Kruczała, K. Operando EPR Study of Radical Formation in Anion-Exchange Membrane Fuel Cells. *ACS Catal.* **2023**, *13* (4), 2744–2750. https://doi.org/10.1021/acscatal.2c05843.
12. Marino, M. G.; Kreuer, K. D. Alkaline Stability of Quaternary Ammonium Cations for Alkaline Fuel Cell Membranes and Ionic Liquids. *ChemSusChem* **2015**, *8* (3), 513–523. https://doi.org/10.1002/cssc.201403022.
13. Ayers, K. E.; Anderson, E. B.; Capuano, C. B.; Niedzwiecki, M.; Hickner, M. A.; Wang, C.-Y.; Leng, Y.; Zhao, W. Characterization of Anion Exchange Membrane Technology for Low Cost Electrolysis. *ECS Trans.* **2013**, *45* (23), 121–130. https://doi.org/10.1149/04523.0121ecst.
14. Tsuneda, T. Fenton Reaction Mechanism Generating No OH Radicals in Nafion Membrane Decomposition. *Sci Rep* **2020**, *10* (1), 18144. https://doi.org/10.1038/s41598-020-74646-0.
15. Koppenol, W. H. Ferryl for Real. The Fenton Reaction near Neutral pH. *Dalton Trans.* **2022**, *51* (45), 17496–17502. https://doi.org/10.1039/D2DT03168J.
16. Wang, Y.; Qiu, J.; Peng, J.; Xu, L.; Li, J.; Zhai, M. Study on the Chemical Stability of the Anion Exchange Membrane of Grafting Dimethylaminoethyl Methacrylate. *Journal of Membrane Science* **2011**, *376* (1–2), 70–77. https://doi.org/10.1016/j.memsci.2011.04.002.
17. Mierzwa, J. C.; Rodrigues, R.; Teixeira, A. C. S. C. UV-Hydrogen Peroxide Processes. In *Advanced Oxidation Processes for Waste Water Treatment*; Elsevier, 2018; pp 13–48. https://doi.org/10.1016/B978-0-12-810499-6.00002-4.
18. Pędziwiatr, P.; Mikołajczyk, F.; Zawadzki, D.; Mikołajczyk, K.; Bedka, A. Decomposition of Hydrogen Peroxide - Kinetics and Review of Chosen Catalysts. *Acta Innovations* **2018**, No. 26, 45–52. https://doi.org/10.32933/ActaInnovations.26.5.
19. Arges, C. G.; Ramani, V.; Wang, Z.; Ouimet, R. J. Assessing the Oxidative Stability of Anion Exchange Membranes in Oxygen Saturated Aqueous Alkaline Solutions. *Front. Energy Res.* **2022**, *10*, 871851. https://doi.org/10.3389/fenrg.2022.871851.
20. Davis, R. E.; Horvath, G. L.; Tobias, C. W. The Solubility and Diffusion Coefficient of Oxygen in Potassium Hydroxide Solutions. *Electrochimica Acta* **1967**, *12* (3), 287–297. https://doi.org/10.1016/0013-4686(67)80007-0.
21. Nemeth, T.; Nauser, T.; Gubler, L. On the Radical-Induced Degradation of Quaternary Ammonium Cations for Anion-Exchange Membrane Fuel Cells and Electrolyzers. *ChemSusChem* **2022**, *15* (22), e202201571. https://doi.org/10.1002/cssc.202201571.
22. Ghassemzadeh, L.; Peckham, T. J.; Weissbach, T.; Luo, X.; Holdcroft, S. Selective Formation of Hydrogen and Hydroxyl Radicals by Electron Beam Irradiation and Their Reactivity with Perfluorosulfonated Acid Ionomer. *J. Am. Chem. Soc.* **2013**, *135* (42), 15923–15932. https://doi.org/10.1021/ja408032p.

© 2025 by the author(s). Distributed under a Creative Commons CC BY license.

Preprints.org (www.preprints.org) | NOT PEER-REVIEWED | Posted: 3 September 2025 doi:10.20944/preprints202509.0371.v1

23. Takeda, K.; Fujisawa, K.; Nojima, H.; Kato, R.; Ueki, R.; Sakugawa, H. Hydroxyl Radical Generation with a High Power Ultraviolet Light Emitting Diode (UV-LED) and Application for Determination of Hydroxyl Radical Reaction Rate Constants. *Journal of Photochemistry and Photobiology A: Chemistry* **2017**, *340*, 8–14. https://doi.org/10.1016/j.jphotochem.2017.02.020.
24. Nosaka, Y.; Nosaka, A. Understanding Hydroxyl Radical (• OH) Generation Processes in Photocatalysis. *ACS Energy Lett.* **2016**, *1* (2), 356–359. https://doi.org/10.1021/acsenergylett.6b00174.
25. Bielski, B. H. J.; Cabelli, D. E.; Arudi, R. L.; Ross, A. B. Reactivity of HO2/O−2 Radicals in Aqueous Solution. *Journal of Physical and Chemical Reference Data* **1985**, *14* (4), 1041–1100. https://doi.org/10.1063/1.555739.
26. Mack, J.; Bolton, J. R. Photochemistry of Nitrite and Nitrate in Aqueous Solution: A Review. *Journal of Photochemistry and Photobiology A: Chemistry* **1999**, *128* (1–3), 1–13. https://doi.org/10.1016/S1010-6030(99)00155-0.
27. Buxton, G. V. Pulse Radiolysis of Aqueous Solutions. Some Rates of Reaction of OH and O? And pH Dependence of the Yield of O ? 3. *Trans. Faraday Soc.* **1969**, *65*, 2150. https://doi.org/10.1039/tf9696502150.
28. Ransdell-Green, E. C.; Baranowska-Kortylewicz, J.; Wang, D. Advances in Fluorescence Techniques for the Detection of Hydroxyl Radicals near DNA and Within Organelles and Membranes. *Antioxidants* **2025**, *14* (1), 79. https://doi.org/10.3390/antiox14010079.
29. Hwang, J. Y.; Moon, G.; Kim, B.; Tachikawa, T.; Majima, T.; Hong, S.; Cho, K.; Kim, W.; Choi, W. Crystal Phase-Dependent Generation of Mobile OH Radicals on TiO2: Revisiting the Photocatalytic Oxidation Mechanism of Anatase and Rutile. *Applied Catalysis B: Environmental* **2021**, *286*, 119905. https://doi.org/10.1016/j.apcatb.2021.119905.
30. Al-Oubidy, E. A.; Kadhim, F. J. Photocatalytic Activity of Anatase Titanium Dioxide Nanostructures Prepared by Reactive Magnetron Sputtering Technique. *Opt Quant Electron* **2019**, *51* (1), 23. https://doi.org/10.1007/s11082-018-1738-z.
31. Wang, J.; Zhao, Y.; Setzler, B. P.; Rojas-Carbonell, S.; Ben Yehuda, C.; Amel, A.; Page, M.; Wang, L.; Hu, K.; Shi, L.; Gottesfeld, S.; Xu, B.; Yan, Y. Poly(Aryl Piperidinium) Membranes and Ionomers for Hydroxide Exchange Membrane Fuel Cells. *Nat Energy* **2019**, *4* (5), 392–398. https://doi.org/10.1038/s41560-019-0372-8.
32. Giovanelli, A.; Pozio, A.; Pucci, A.; Geppi, M.; Martini, F. Fumasep FAA-3-PK-130: Exploiting Multinuclear Solid-State NMR to Shed Light on Undisclosed Structural Properties. *Polymer* **2024**, *311*, 127536. https://doi.org/10.1016/j.polymer.2024.127536.
33. Mandal, M.; Huang, G.; Kohl, P. A. Highly Conductive Anion-Exchange Membranes Based on Cross-Linked Poly(Norbornene): Vinyl Addition Polymerization. *ACS Appl. Energy Mater.* **2019**, *2* (4), 2447–2457. https://doi.org/10.1021/acsaem.8b02051.
34. Buxton, G. V.; Greenstock, C. L.; Helman, W. P.; Ross, A. B. Critical Review of Rate Constants for Reactions of Hydrated Electrons, Hydrogen Atoms and Hydroxyl Radicals (·OH/·O− in Aqueous Solution. *Journal of Physical and Chemical Reference Data* **1988**, *17* (2), 513–886. https://doi.org/10.1063/1.555805.
35. Buxton, G. V.; Wood, N. D.; Dyster, S. Ionisation Constants of ˙OH and HO˙2 in Aqueous Solution up to 200 °C. A Pulse Radiolysis Study. *J. Chem. Soc., Faraday Trans. 1* **1988**, *84* (4), 1113. https://doi.org/10.1039/f19888401113.
36. Anbar, M.; Meyerstein, D.; Neta, P. The Reactivity of Aromatic Compounds toward Hydroxyl Radicals. *J. Phys. Chem.* **1966**, *70* (8), 2660–2662. https://doi.org/10.1021/j100880a034.
37. Bao, Z.-C.; Barker, J. R. Temperature and Ionic Strength Effects on Some Reactions Involving Sulfate Radical [SO_4^- (Aq)]. *J. Phys. Chem.* **1996**, *100* (23), 9780–9787. https://doi.org/10.1021/jp9603703.
38. Buxton, G. V. Pulse Radiolysis of Aqueous Solutions. Rate of Reaction of OH with OH? *Trans. Faraday Soc.* **1970**, *66*, 1656. https://doi.org/10.1039/tf9706601656.
39. Guo, L.; Masuda, A.; Miyatake, K. Reinforcement Effect in Tandemly Sulfonated, Partially Fluorinated Polyphenylene PEMs for Fuel Cells. *RSC Adv.* **2023**, *13* (16), 11225–11233. https://doi.org/10.1039/D3RA01041D.
40. Clemens, A. L.; Jayathilake, B. S.; Karnes, J. J.; Schwartz, J. J.; Baker, S. E.; Duoss, E. B.; Oakdale, J. S. Tuning Alkaline Anion Exchange Membranes through Crosslinking: A Review of Synthetic Strategies and Property Relationships. *Polymers* **2023**, *15* (6), 1534. https://doi.org/10.3390/polym15061534.

© 2025 by the author(s). Distributed under a Creative Commons CC BY license.

Preprints.org (www.preprints.org) | NOT PEER-REVIEWED | Posted: 3 September 2025 doi:10.20944/preprints202509.0371.v1

41. Lewis, R. S.; Deen, W. M. Kinetics of the Reaction of Nitric Oxide with Oxygen in Aqueous Solutions. *Chem. Res. Toxicol.* **1994**, *7* (4), 568–574. https://doi.org/10.1021/tx00040a013.
42. Uchino, T.; Tokunaga, H.; Ando, M.; Utsumi, H. Quantitative Determination of OH Radical Generation and Its Cytotoxicity Induced by TiO2–UVA Treatment. *Toxicology* in Vitro **2002**, *16* (5), 629–635. https://doi.org/10.1016/S0887-2333(02)00041-3.

Disclaimer/Publisher's Note: The statements, opinions and data contained in all publications are solely those of the individual author(s) and contributor(s) and not of MDPI and/or the editor(s). MDPI and/or the editor(s) disclaim responsibility for any injury to people or property resulting from any ideas, methods, instructions or products referred to in the content.

© 2025 by the author(s). Distributed under a Creative Commons CC BY license.